A New Paradigm in High-Speed and High-Efficiency Silicon Photodiodes for Communication—Part I: Enhancing Photon–Material Interactions via Low-Dimensional Structures

Hilal Cansizoglu, *Member, IEEE*, Ekaterina Ponizovskaya Devine, Yang Gao, Soroush Ghandiparsi, Toshishige Yamada, *Senior Member, IEEE*, Aly F. Elrefaie, *Fellow, IEEE*, Shih-Yuan Wang, *Life Fellow, IEEE*, and M. Saif Islam, *Senior Member, IEEE*

(Invited Review Paper)

***Abstract*— Photodetectors (PDs) used in communication systems require ultrafast response, high efficiency, and low noise. PDs with such characteristics are increasingly in demand for data centers, metro data links, and long-haul optical networks. In a surface-illuminated PD, high speed and high efficiency are often a tradeoff, since a high-speed device needs a thin absorption layer to reduce the carrier transit time, whereas a high-efficiency device needs a thick absorption layer to compensate for the low absorption coefficient of some semiconductors such as Si and Germanium (Ge) or SiGe alloys at wavelengths near the bandgap. In this part of this review, we present the recent efforts in enhancing the photon–material interactions by using low-dimensional structures that can control light for more interaction with the photoabsorbing materials, slow down the propagation group velocity and reduce surface reflection. We present recent demonstrations of high-speed PDs based on nanostructures enabled by both synthetic bottom-up or transformative top-down processing methods. In particular, we detail a CMOS-compatible ultrafast surface-illuminated Si PD with 30-ps full-width at half-maximum, and >50% efficiency at 850 nm. A complementary discussion on device challenges and the integration of low-dimensional structures will be presented in the part II of this review.**

Manuscript received October 10, 2017; revised November 23, 2017; accepted November 24, 2017. Date of publication December 18, 2017; date of current version January 22, 2018. This work was supported in part by S. P. Wang and S. Y. Wang Partnership, in part by Army Research Office under Grant W911NF-14-4-0341, and in part by the National Science Foundation under Grant CMMI-1235592. The review of this paper was arranged by Editor C. Surya. *(Corresponding author: Hilal Cansizoglu.)*

H. Cansizoglu, Y. Gao, S. Ghandiparsi, and M. S. Islam are with the Integrated Nanodevices and Nanosystem Research Group, Department of Electrical and Computer Engineering, University of California, Davis, CA 95616 USA (e-mail: hcansizoglu@ucdavis.edu; sislam@ucdavis.edu).

E. Ponizovskaya Devine, A. F. Elrefaie, and S.-Y. Wang are with W&WSens Devices, Inc., Los Altos, CA 94022 USA (e-mail: sywang@ieee.org).

T. Yamada is with the Baskin School of Engineering, University of California, Santa Cruz, CA 95064 USA (e-mail: tyamada@soe.ucsc.edu).

Color versions of one or more of the figures in this paper are available online at http://ieeexplore.ieee.org.

Digital Object Identifier 10.1109/TED.2017.2779145

***Index Terms*— High-efficiency photodetectors (PDs), high speed, light trapping, nanostructures, photon absorption, photon–material interaction, slow light.**

I. Introduction

HIGH-SPEED photodetectors (PDs) for communication convert optical signals (photons) into electrical signals (electrons and holes). There are two important factors determining PDs' performance: 1) how effectively electrons and holes are generated and 2) how good the carrier (electron and hole) transport is. Once a particular semiconductor material is chosen (for instance, silicon), the carrier transport properties remain unchanged—mostly limited by the carrier mobility of the semiconductor. One can only explore new methods for improving the electron–hole (e–h) pair generation and collection efficiency. Most common device structure in high-speed PDs involves p-i-n diode (i.e., intrinsic layer, or i-layer, sandwiched between highly doped p and n layers serving as contacts). Photoconductive mode of p-i-n diodes, which requires a reverse bias of moderate magnitude, is the common configuration in high-speed PDs. The thickness of the i-layer determines the transit time that is required for carriers to reach the contacts. For ultrafast operations, the i-layer needs to be thin enough to ensure sufficiently high bandwidth. However, a thin i-layer cannot efficiently absorb the incoming photons. This leads to a tradeoff between efficiency and speed in the conventional p-i-n diodes.

There is a longstanding belief that most common materials used in semiconductor manufacturing such as Si cannot be employed in designing a surface-illuminated PD for ultrahigh-speed communication networks due to their low absorption coefficients at near-infrared wavelengths such as 850 nm—a wavelength commonly used for short-reach optical communication. A number of absorption enhancement methods without using a thick i-layer have been applied to surface-illuminated Si PDs for high-speed operations.

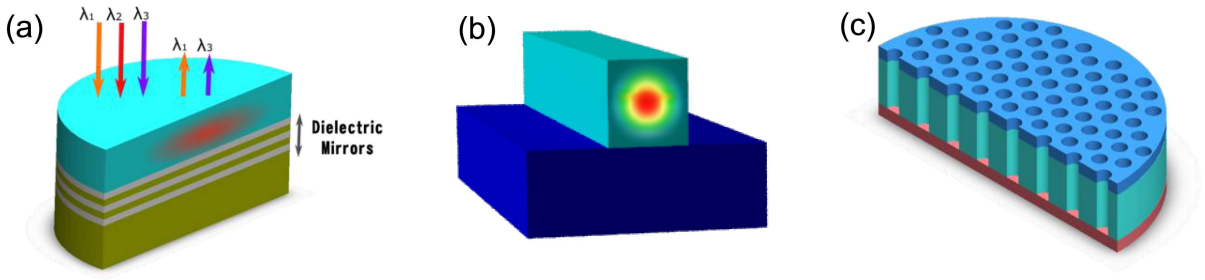

Resonant Cavity Enhanced PD	Waveguide PD	Holes integrated PD
Surface-illuminated	Edge-coupled	Surface-illuminated
Narrow optical bandwidth	Broadband	Broadband
Requires careful design/ fabrication of dielectric mirrors	Tight fiber alignment tolerance	CMOS compatible

Fig. 1. (a) Resonant cavity-enhanced PD with high bandwidth and wavelength-dependent high quantum efficiency. (b) Waveguide PD that confines light in a thin and long absorption region and the electrical signal is collected in a transmission line as light propagates forward. High-precision alignment of fiber contributes to high packaging cost in such a device. (c) Holes integrated in a PD fabricated via CMOS compatible process for low reflection, broadband absorption, high efficiency, and high bandwidth.

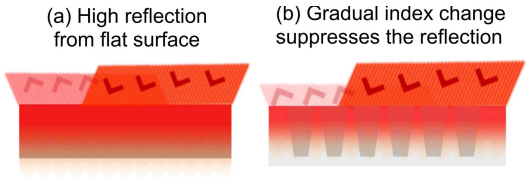

Fig. 2. (a) High reflection from planar surface requires additional ARCs on photodetectors. (b) Gradual refractive index change with funnel-shaped holes suppresses surface reflection and eliminates ARC.

Prior work in high-speed Si PDs mainly involved surface-illuminated resonant cavity enhanced (RCE) PDs and edge-illuminated waveguide PDs, as depicted in Fig. 1(a) and (b), respectively. In the RCE PD, the optical path is prolonged due to multiple passes of light supported by the cavity [1], [2]. This makes RCE PD to have high external quantum efficiency (EQE); however, the useful optical bandwidth is narrow. This limits the practicality of RCE PD since the optical source wavelengths need to match the detector wavelength within a few nanometers [1]. In addition, any thermal drift of the laser wavelength can result in a decrease in sensitivity at the optical receiver. On the other hand, optical links in data centers are typically not temperature controlled and the temperature can fluctuate by 40 °C or more. This also limits RCE PDs from being practically used in optical receivers. Alternatively, waveguide Si PDs [3]–[6] can have both high EQE and high speed. Long absorption lengths along the waveguide enable high EQE and thin intrinsic layer allows short e–h transit time since the optical wave propagation direction is perpendicular to the electric field. However, waveguide PDs require precision packaging for efficient coupling of a single-mode optical fiber to the optical waveguide, resulting in high packaging costs [7], [8]. A technology that enables a surface-illuminated PD with an ultrathin absorption layer to absorb majority of the incident photons is highly desirable to address the tradeoff between efficiency and bandwidth.

There has been a lack of practical high-speed Si PDs until the recent demonstration of a CMOS-compatible, high-efficiency, and high-speed Si PD [9] with integrated photon-trapping micro-/nanoholes. In such a PD depicted in Fig. 1(c), vertically oriented incoming photon beams with a direction of propagation parallel to the axis of the holes interact with the holes to generate both vertically and laterally propagating modes and allow them to interact with Si for a prolonged time until they are efficiently absorbed. This approach can overcome the weak absorption coefficient of Si at the datacom wavelengths between 800 and 950 nm.

The first part of this review will present an overview of the applications of photon-trapping structures in PDs and the recent device demonstrations with low-dimensional structures. The aim of this review is to illustrate current stage of the micro-/nanostructured PDs for high-speed communications and offer readers a perspective on practical solutions for high-efficiency and ultrafast PDs with photon-trapping structures. The second part will discuss device design challenges and the integration of photon-trapping structures.

A. Applications of Photon Manipulating Structures in PDs

Besides the weak absorption, the Si surface reflects around 30% of light. Antireflection coatings (ARCs) are usually used to reduce the reflection at the air–Si interface. However, ARCs fabricated with conventional methods are wavelength dependent and thus do not suppress reflection of light with a wide-spectral range and impinging with wide incident angles. Even though the ARC is designed to reduce the reflection at the air–Si interface, Si is still a less attractive material to absorb light at longer wavelengths. On the other hand, light can be manipulated by introducing the micro-/nanostructures in the material. Broader discussion on nanostructures designed for optoelectronic devices can be found in [10]. This part of this review will focus on the applications of micro-/nanostructures

in high-speed PDs regarding the optical properties of the active PD materials.

1) Inhibiting Broadband Reflection: The nanostructures at the surface of the material dramatically change the interaction of light at the air–material interface. Due to porosity introduced by the nanostructures, the effective refractive index of the air–material matrix is lower than the refractive index of the bulk material without nanostructures. Thus, the difference of refractive indices of air and the material at the air–material interface, where most of the reflection happens [Fig. 2(a)], decreases, and results in reduced reflection. The structures with hierarchical geometry such as tapered pillars/holes, funnels, cones, needle-like wires, and pyramids cause even lower reflection [Fig. 2(b)] by introducing graded refractive index and thus providing a broadband antireflective coating [11]. Graded-refractive-index coatings include multilayer structures with different refractive indexes or moth-eye like structures, such as subwavelength arrays of nanoparticles. The graded-index antireflection coating is designed to match the impedance at the surface for broad range of wavelengths. Tapered pillars/holes compose a layer of an effective refractive index that gradually increases from the top to the bottom of the structure, providing broadband impedance matching. In addition, shapes such as funnel or inverse pyramid with dimensions larger than the wavelength of incoming light reduces the reflection due to the better coupling of the incident light into the modes that are supported by the structure [9].

2) Broadband Absorption Enhancement by Photon Manipulations and Slow Light: Many studies [12]–[18] that have demonstrated the absorption enhancement in surface-illuminated semiconductors with micro-/nanostructures mostly focused on photovoltaics applications. Although the dimensions of the structures are not optimized for datacom wavelengths, high-efficiency solar cells with a broadband absorption can benefit the development of surface-illuminated high-speed and high-efficiency PDs. For high-speed operation (bandwidth >1 GHz), the intrinsic absorption layer must be less than 10 μm. Table I shows the recent demonstrations of enhanced absorption in Si with ≤ 10 μm thickness and with integrated micro-/nanostructures in the case of incident light parallel to the micro-/nanostructure axis. The data presented in Table I are for the wavelength range of 800–900 nm. Clearly, the textured surfaces exhibit high absorption with very thin Si layer.

The well-known theory of light trapping establishes that absorption enhancement in a medium cannot exceed the factor of $4n^2/\sin^2\theta$, where n is the refractive index of the active layer, and this factor is known as the Lambertian or Yablonovitch limit [19]. The limit can be exceeded [20] using nanostructures, where the wavelength of the incident light is comparable to the dimensions of these structures [21] leading to new understanding of this phenomenon such as Mie scattering, guided resonaces, statistical temporal coupled mode theory, parallel interface refraction, and light manipulation in high-contrast gratings [22].

Mie scattering considers nanostructures as particles that redirect, absorb, and reradiate the incident light, where the refractive index mismatch between particle and medium is as important as the dimensions of the particle and the wavelength of light in the medium [23]. However, light can scatter in a wide angle and can cause loss in the PDs of interest, which must confine light in the absorbing layer. Meanwhile, guided resonances in a photonic crystal (PC) slab [24], [25] can couple into the incident light and enhance the absorption for certain frequencies. The statistical temporal coupled mode theory [26] has been developed to describe the collection of such modes for broadband absorption. The mode analysis of the guided mode resonance was done in [27], which shows an increase in absorption due to a resonance of the guided mode in the periodic structures. With an optimized design, one can confine light in the absorbing i-layer and maximize the absorption. The leaky modes in the PC slab can be useful too for the absorption of light if the length of the propagation ($1/\mathrm{Im}(k_c)$, where k_c is the propagation constant) inside the slab before it would leak out, is longer than $1/\alpha$ (where α is the absorption coefficient of the material).

The slow light effects have been examined in photonic crystals (PC) and photonic crystal waveguides (PCWs) where the group velocity (u_g) can be significantly smaller than that in the uniform material due to the photons scattering on the periodic structure. Such effect was observed at the PC's band gap edges and in PCW with large first order dispersion $dk/d\omega$, which is the inverse group velocity ($1/u_g = dk/d\omega$), where k is the wave vector and ω is the light frequency. However, vertically illuminated light cannot excite these modes and therefore they are not applicable for surface-illuminated PDs.

TABLE I
COMPARISON OF ABSORPTION OF SI WITH SURFACE TEXTURING

Structure shape	Absorption	Layer thickness (μm)	Fabrication method
Teepee-like [12]	96 % (A*)	10	Top-down (dry-RIE)
Si cones [13]	60-70 % (EQE**)	10	Top-down (dry-RIE)
Light trapping structures with anti-reflection coating and back reflection layer [14]	60-70 % (A*)	3	Top-down (dry-RIE)
2D inverted pyramid photonic crystal and a rear dielectric/reflector stack [15]	90-95 % (A*)	10	Top-down (wet-KOH)
Nanorods and nanopencils [16]	>95% (A)	NA	Top-down (wet etch)
Nanowires[17]	5% solar cell efficiency	8	Top down (dry-DRIE)
Nanodome with Ag back reflector[18]	94% (A*) and 5.9% solar cell efficiency	0.28	Top down (dry-RIE)

*"A" stands for absorption of light.
** EQE is external quantum efficiency.
The presented data is for λ=800-900 nm.

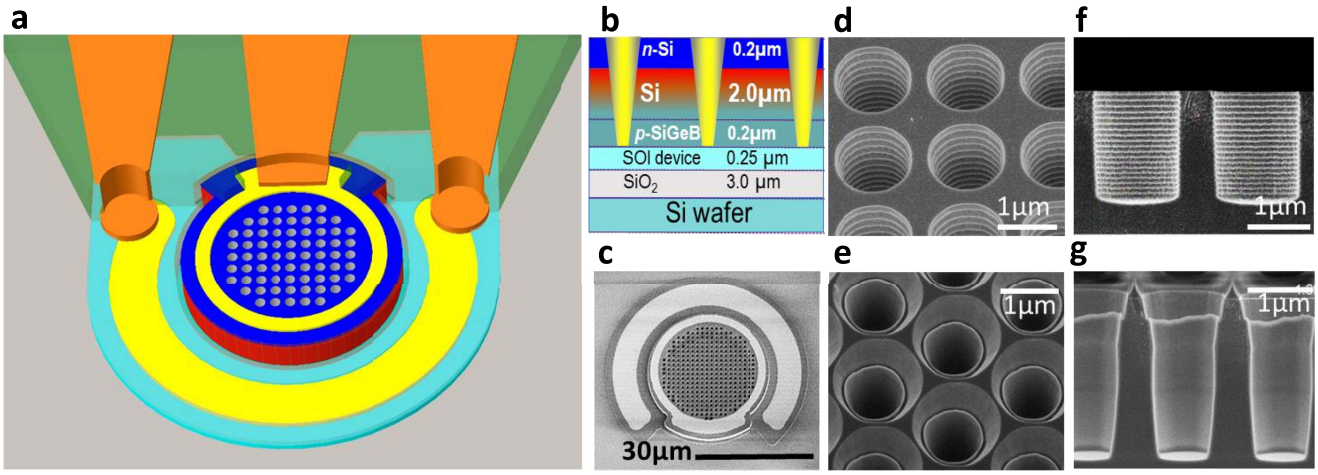

Fig. 3. (a) Schematic of the ultrafast photodiode with a thin absorbing region. Color-coded layers are blue: *n*-Si layer, red: *i*-Si layer, turquoise: *p*-Si layer, transparent: insulating nitride/oxide layer, yellow: ohmic metal, brown: high-speed coplanar waveguide (CPW) contacts, and green: polyimide planarization layer. (b) n-i-p PD structure on an SOI wafer showing the integrated tapered holes that span the n-, i-, and p-layers. (c) SEM micrograph of the active region of a high-speed PD with 30-μm diameter. (d) Square and (e) hexagonal hole lattice integrated in the PDs. Cross section of (f) cylindrical- and (g) funnel-shaped or tapered holes etched into the active photodiode regions (reproduced by permission of Nature Publishing Group from [9]).

Sturmberg *et al.* [28] calculated low group velocities for the longitudinal modes in Si nanowire arrays where the absorption is increased due to the higher intensities in the slow light regions. Sakoda [29] has also shown light amplification in a PC with air holes due the longitudinal slow modes with small group velocities [29]. However, such longitudinal slow modes can be excited at a discrete set of frequencies and they are subject to the layer thickness and the periodicity; therefore, they may not be useful for broadband absorption enhancement in surface-illuminated high-speed PDs. On the other hand, lateral traveling modes with low group velocities have been observed in surface-illuminated Si with the funnel shaped holes [9]. This helps light dwell in the *i*-layer longer time and get almost fully absorbed despite a very thin absorbing layer that determines the speed of the PD. The longer the dwell time for the lateral modes (near-parallel to the active layer), the better is the absorption for a wide range of wavelengths. The 3-D structures with 2-D periodicity that have inclined side walls such as teepee-like structures [12], cones [30]–[32], or inverted pyramids [15] embedded in dielectric material have already been demonstrated to provide broadband absorption. In addition, elliptical holes [33] and aperiodic [34] or random holes have been proposed to promote broadband absorption and experimentally [35] shown for improved broadband absorption for photovoltaics. These structures can be integrated to surface-illuminated PDs for broadband high efficiency.

II. Recent Device Demonstrations

A. Ultrafast and Highly Efficient Surface-Illuminated Broadband Silicon Photodiodes With Photon-Trapping Micro-/Nanostructures

Recently, a high-efficiency and high-speed silicon PD with 52% EQE has been demonstrated for 20 Gb/s data rate operation using photon-trapping micro-/nanostructures on Si surface [9]. The schematic and scanning electron microscopy images of the holes integrated Si PD are shown in Fig. 3(a)ãnd (c), respectively. The micro-/nanoholes on the silicon surface enable light trapping and enhance the absorption of silicon by an order of magnitude (compared to flat surface silicon PDs) with the generation of the lateral modes at the wavelengths between 800 and 900 nm. On the other hand, the ultrathin "intrinsic" silicon layer as indicated in Fig. 3(b) can reduce the transit time of the *e*–*h* pairs generated in that region and ensure an ultrafast response of the PD device. In this review, the cylindrical [as shown in Fig. 3(d) and (f)] and funneled holes [as shown in Fig. 3(e) and (g)] were patterned by deep ultraviolet lithography, and then etched by deep reactive ion etch (DRIE) and reactive ion etch (RIE), respectively. In this process, DRIE uses alternating cycles of etching based on sulfur hexafluoride (SF_6) gas and protective polymer deposition based on octafluorocyclobutane (C_4F_8) gas to achieve vertical high aspect ratio etch. RIE is based on chlorine (Cl_2) and hydrogen bromide gasses, and the thickness and profile of the photoresist was used to control the sidewall angle of the etched holes. Next, DRIE was used to form the PD mesa. Ohmic metal rings which consist of 100 nm of Al and 20 nm of Pt are deposited by sputtering. These methods are CMOS compatible and do not require the expensive integration of photonic and electronic devices as GaAs, InGaAs/InP PDs normally do, and have great potential to reduce the cost by 30% or more than the current technologies based on III–V materials offer. To suppress the leakage current associated with the dry etch damages caused on the silicon surface, hydrogen fluoride (HF) dip was applied after the holes are created. HF provides hydrogen termination to the dangling bonds of silicon surface induced by dry etch, and can successfully reduce the dark current by more than an order of magnitude [9], [36].

The lateral mode formation is shown in Fig. 4 (with Poynting vector). The Poynting vector was simulated using finite-difference time-domain method, and shows the energy flow along the surface.

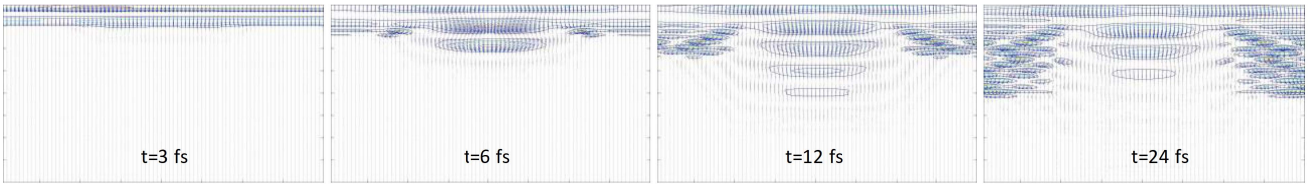

Fig. 4. Cross-sectional views of Poynting vectors under vertical optical illumination. The Poynting vectors in the cross-sectional view of a hole in time (from the left to the right as $t = 3$, 6, 12, and 24 fs). The Poynting vector is directed from the holes into silicon indicating that the energy propagates outward from the holes and is trapped in silicon until it is mostly absorbed.

As shown in Fig. 5(a), the funnel shape holes offer advantages over cylindrical holes in terms of the absorption. The effective refractive index gradually changes from the surface through the Si with funnel-shaped holes compared to the cylindrical holes that have abrupt change of the refractive index. Thus, the funnel-shaped holes create an effect like a graded-refractive-index ARC.

Due to the photon-trapping mechanism enabled by the micro-/nanoholes, the EQE of the all-silicon PD has been greatly improved. The measured EQE of Si PD with micro-/nanostructures was 52% at 850 nm, compared to 6% of a flat device as shown in Fig. 5(a). On the other hand, the improvement of the absorption can allow the PD to be made thinner than 2 μm, which is less than 1/5 of the thickness of the conventional silicon photodiodes for similar EQE. As shown in Fig. 5(b), the full-width at half-maximum (FWHM) response of the micro-/nanoholes-based PD is 30 ps, equivalent of an ultrafast data transmission rate of >20 Gb/s. A residual photocurrent tail observed in the pulse response in Fig. 5(b) is believed to be caused by the slow diffusion of photogenerated minority carriers in p- and n-layers where the doping profile is soft and not abrupt with the i-layer. Growth of more abrupt p-i and i-n interfaces must minimize the slow diffusion tail.

Recently, light-trapping inverted pyramids similarly enhance the absorption in a Si single-photon avalanche photodiode (SPAD) [37].

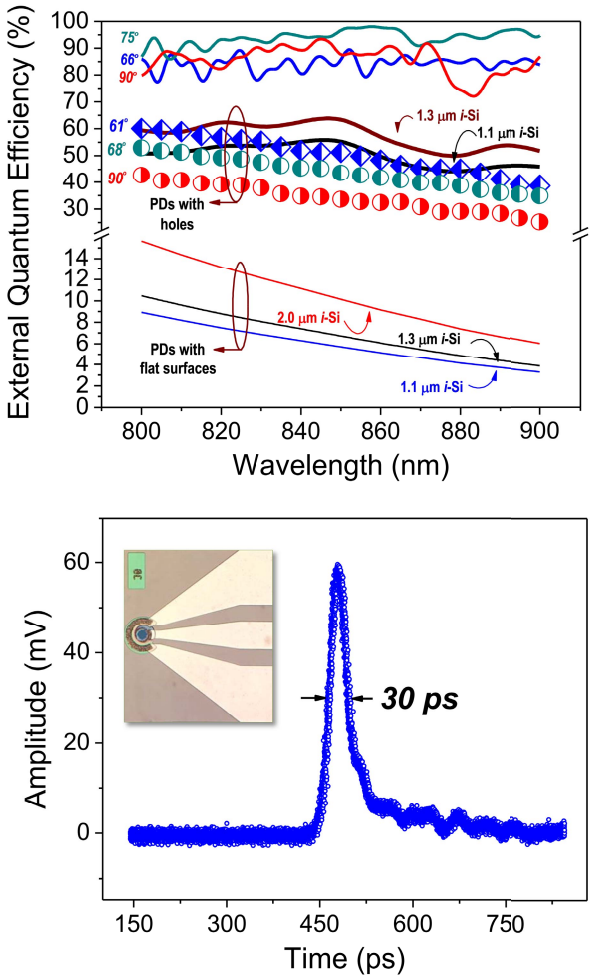

Fig. 5. (a) (Top lines) Absorption (1-R-T)calculated in a p-i-n stack that includes p and n contact layers as well as the absorbing *i*-Si layer along with holes etched in funnel shapes with angles of 75°, 66°, and cylindrical shapes (90°). Experimentally measured EQE versus wavelengths for PDs with integrated holes that have a diameter of 700 nm and a period of 1000 nm in funnel shapes with angles of 61°, 68°, and cylindrical shapes (90°). The measured EQEs were above 62% at 800 nm and 52% at 850 nm. The simulation results (black and blue lines at the top) show that our PDs with holes have an absorbing *i*-Si layer thickness between 1.1 and 1.3 μm, although the design thickness was 2 μm. Such reduced thickness was also corroborated by capacitance–voltage measurements. (Bottom lines) Absorption calculated absorbing *i*-Si layer with 1.1-, 1.3-, and 2-μm thickness. (b) By illuminating a PD with a subpicosecond pulse, a 30-ps FWHM response was observed by a 20-GHz oscilloscope, which is a measurement setup limited response. When corrected for the oscilloscope bandwidth and laser pulse width, the device temporal response is estimated to be 23 ps at 850 nm. Inset: Optical micrograph of a device with a high-speed CPW transmission line (reproduced by permission of Nature Publishing Group from [9]).

B. Photodetectors With Integrated Nanowires

Nanowire PDs have been studied extensively during the evolution of nanofabrication techniques. The reader can find broad [38]–[40] or focused reviews [41], [42] on nanostructure integrated PDs. The discussion in this section is limited to "ultrafast" PDs with integrated nanowires. However, recent demonstrations of high-speed nanowire PDs are scarce. Table II presents nanowire/pillar integrated ultrafast III–V PDs, and recent demonstrations of high-speed Si PD with micro-/nanoholes and Si SPAD with inverted pyramids. Logeeswaran *et al.* [43] demonstrated a 14-ps FWHM photoconductor with intersecting InP nanowires illuminated with a pulse laser at 780 nm. As mentioned above, one of the great challenges of nanowire devices is the ohmic contact formation due the characteristics of metal–nanowire interface. The unique fabrication technique of bridged nanowires [44], [45] utilized in this review enables self-welded and naturally ohmic contacts and allows the nanowires fabrication implemented in traditional contact processes. Gallo *et al.* [46] report metal–semiconductor–metal PDs with Schottky-contacted GaAs/AlGaAs core/shell nanowires with a 5-ps FWHM pulse response, higher than the response that bare core nanowires exhibit. However, the responsivity of this type PDs is quite low due to the lack of efficient light coupling to extremely small

TABLE II
HIGH-SPEED NANOWIRE PDS FOR TELECOM AND DATACOM APPLICATIONS

Material system	Device type	Responsivity	λ (nm)	Pulse Response or Bandwidth
Si with micro-/nanoholes [9]	vertical pin diode	0.36 A/W	850	30 ps (FWHM)
InP nanowires [43]	Photo-conductor	0.3 A/W	780	14 ps (FWHM)
GaAs/ AlGaAs core/shell nanowire [46]	MSM with Schottky contacts	0.1 mA/W	800	5 ps (FWHM)
GaAs nanowires [47]	Schottky-like junction	0.65 A/W	850	9 GHz
InGaAs nanopillar [48]	avalanche	NA	1060	201GHz (GBP*)
Si-plasmonics [49]	MSM	0.12 A/W	1550	40 GHz
Nano-structured Si [37]	SPAD	32% PDE**	850	25 ps (FWHM)

*Gain-bandwidth product.
**Photon detection efficiency.

active area. For this reason, arrays of nanowires can be more practical for surface-illuminated PDs. For example, GaAs nanowire-array PD with large active area demonstrated in [47] has 0.65 A/W responsivity at 850 nm. In this review, indium tin oxide was sputtered on 50-μm active area of GaAs nanowires filled with hydrogen silsesquioxane. Large active area resulted in higher responsivity due to efficient light coupling. In [48], InGaAs nanopillar-based avalanche photodiodes (APDs) are demonstrated. Such PDs exhibit 200-GHz gain-bandwidth product while operated at 1060-nm wavelength of light.

C. Recent Advances in Plasmonics for Photodetectors

Recent studies have demonstrated that the utilization of plasmonic nanostructures can be a promising alternative technology to achieve light trapping in thin-film PDs [50], [51]. Surface plasmons (SPs) are the oscillations of free electron gas coupled to electromagnetic waves at the surface of conductors. SP polaritons (SPPs) propagate on the interface of planar metal and semiconductor, on the other hand, localized SP resonances (LSPRs) are bounded to the surface of a nanoparticle [52]. Plasmonic nanostructures enhance light trapping in different mechanisms; metallic nanoparticles which act as subwavelength scattering centers, can couple the incident light by folding it into the semiconductor [Fig. 6(a)]. In addition, nanoparticles embedded in the film, acting like a subwavelength nanoantenna, can cause coherent electromagnetic energy transport along the absorbing material by means of

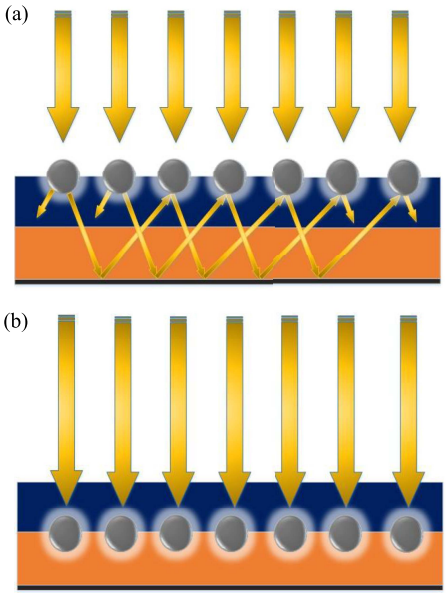

Fig. 6. (a) Light trapping by scattering from metal nanoparticles at the surface. (b) Light trapping by exciting plasmon polaritons embedded at the interface of semiconductors.

strong near-field coupling of plasmon oscillations between nanoparticles [Fig. 6(b)] [53].

Excited SPPs due to photon absorption can decay rapidly (few femtoseconds) [54] through a radiative or nonradiative process. Radiation is followed by internal photoemission while nonradiative mechanism leads to generation of high-energy electrons, known as "hot electrons." Transition of electrons with sufficient energy across the Schottky barrier leads to photocurrent generation [55], [56]. Narang *et al.* [57] have illustrated that SPs can considerably improve the generation and extraction of efficient hot electrons and increase the quantum efficiency of the device.

Conventional mid-wave infrared PDs have low efficiency near room temperature. Ishi *et al.* [58] have fabricated a silicon Schottky nanophotodiode with SP antenna to increase photocurrent considerably. In addition, plasmonics have been used to enhance light concentration into small-volume PDs for various high-speed and high-sensitivity applications such as chip scale optical communications [59]–[62].

Goykhman *et al.* [59] have demonstrated an on-chip integrated metal graphene–silicon plasmonic Schottky PD with 85 mA/W responsivity at 1.55 μm and 7% internal quantum efficiency. Such PD can operate in high-speed (tens of gigahertz) regime. By inserting a graphene monolayer at the metal–semiconductor interface, graphene-based plasmonic PD has achieved high internal quantum efficiency [59]. The new PD's quantum efficiency is one order of magnitude higher than previously reported metal–silicon Schottky PDs operated at 1.55 μm [63]. Recently, a Si plasmonic waveguide detector, which utilized internal photoemission mechanism, has been demonstrated for 40 Gb/s data transmission rate with 0.12 A/W responsivity at 1550-nm wavelength [49]. Such developments can lead very small-scale PDs that can be integrated to Si photonics circuits.

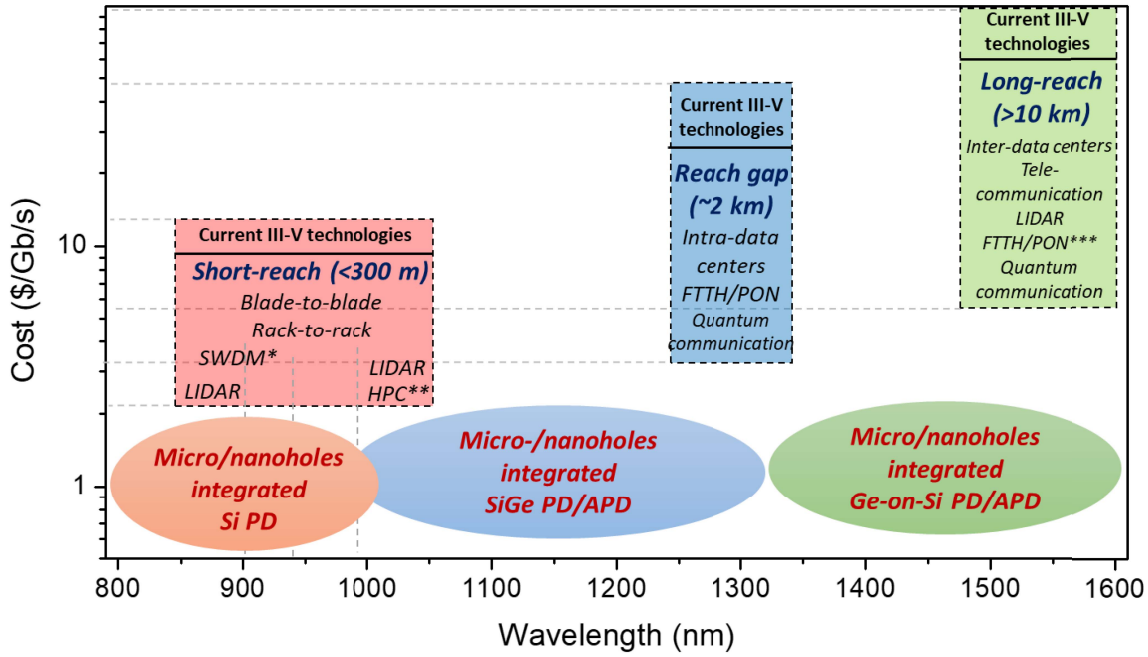

Fig. 7. Illustration of cost ($/Gb/s) and wavelength range of various applications that require high-speed transceivers with the current III–V technologies packaged with TIA or clock and data recovery circuits and other necessary electronics and used in current ROSA (receiver optical subassembly). CMOS integration of Si, SiGe, and Ge-on-Si PDs, and APDs with micro-/nanoholes can lower the transceiver cost to single digit $/Gb/s by bypassing the cost of packaging with the electronics. *Short wavelength division multiplexing. **High-performance computing. ***Fiber to the home/passive optical network. Inset: Schematics of a p-i-n photodiode and an APD with photon-trapping holes in the active region.

III. Conclusion

Light Manipulation Could Bring About a Paradigm Shift in the Design of High-Speed and High-Efficiency Photodetectors

The developments in the theoretical concept and the fabrication of photonic crystals in the last two decades were not employed by the PD community. Research has mainly focused on the bandgap of photonic crystals for applications including waveguides, couplers, and modulators for photonic integrated circuits [64]. In addition, innovations in photonic crystals contributed to photonic crystal fibers [65] for near-zero dispersion, where the intrinsic dispersion of the material is compensated by the waveguide dispersion. Photon manipulation by photonic crystals or surface textures to increase the optical absorption has recently been studied mostly targeting photovoltaics applications [12]–[15], [66]. Device fabrication, passivation, and integration challenges that need to address high dark current or persistent photocurrent of nanostructured PDs prevented implementation of photonic crystals or surface texturing into PDs until recently. In addition, the difficulty to make electrical contacts to such devices further escalated the problem. Structures with high surface to volume ratios commonly suffer from high density of surface states causing carrier-trap centers, resulting in high leakage current, persistent photocurrent, and long diffusion induced tail in the PD electrical output. All these issues demand special attention to the device fabrication and the surface passivation schemes in the process lines. Several novel designs for light trapping are developed to utilize the conventional processes for the fabrication of electrical contacts [9], [37], [67]–[70]. For example, arrays of negative structures such as holes, cones, and pyramids are more advantageous since they do not require individual contacts [9], [37] as opposed to the arrays of positive structures such as pillars, wires, and rods [67]–[70]. The drawbacks and device integration challenges of nanostructures will be reviewed and discussed in detail in the part II of this review.

New insights in the light-trapping mechanisms can now be implemented in PDs to develop a new generation of ultrafast Si PDs [9], [71]. Fig. 7 is intended to give a perspective to the reader about potential applications that can be transformed by Si-based PDs with integrated micro-/nanostructures. One possible application is light detection and ranging systems (LIDAR) used in autonomous vehicles. The optical transmitters in such systems use semiconductor laser diodes emitting at 850 or 905 nm [72]. In addition, a single wavelength operation at 850 nm commonly used for short-reach optical data communication cannot meet the needs of a modern data center due to increasing data rates of 10, 25, 50, 100 Gb/s and beyond. Short wavelength division multiplexing, which allows 4–5 wavelength ranges piped into a multimode optical fiber, can be a solution to this challenge [73], [74]. The wavelengths can be chosen from 850 to 940 nm, e.g., 850, 880, 910, and 940 nm, as stated by multisource agreement for 100 Gb/s Ethernet application [75]–[77]. In addition, 980 nm has been proposed, thanks to the advancements of Er-doped fiber laser technology [76]. High-efficiency and high-speed Si PDs with photon-trapping structures can be a part of the solution to the demand for high data transmission rate for the applications mentioned above. CMOS-compatible processes will enable the monolithic integration of PDs with ICs and can drastically

lower the cost of the transceivers by eliminating the packaging and additional processing cost. Furthermore, operating wavelengths for high-performance computing (HPC) [78], which is another application area that requires high-speed and high-efficiency PDs, cover 990, 1015, 1040, and 1065 nm [77]–[79]. For practical PDs for HPCs, alloys of SiGe can be chosen as absorption layer with photon-trapping structures (Fig. 7). Si, Si/Ge, and Ge-on-Si PDs integrated with micro-/nanoholes have potential to replace costly InGaAs/InP-based PDs for short- and long-reach communications at intra- and interdata centers, fiber to the home, passive optical networks [80], LIDAR [81], [82], and quantum communication systems [83].

REFERENCES

[1] M. S. Ünlü, M. K. Emsley, O. I. Dosunmu, P. Muller, and Y. Leblebici, "High-speed Si resonant cavity enhanced photodetectors and arrays," *J. Vac. Sci. Technol. A, Vac. Surf. Films*, vol. 22, no. 3, pp. 781–787, May 2004, doi: 10.1116/1.1647591.

[2] E. Ozbay *et al.*, "Fabrication of high-speed resonant cavity enhanced Schottky photodiodes," *IEEE Photon. Technol. Lett.*, vol. 9, no. 5, pp. 672–674, May 1997, doi: 10.1109/68.588199.

[3] J. J. Ackert, A. S. Karar, J. C. Cartledge, P. E. Jessop, and A. P. Knights, "Monolithic silicon waveguide photodiode utilizing surface-state absorption and operating at 10 Gb/s," *Opt. Exp.*, vol. 22, pp. 10710–10715, Apr. 2014, doi: 10.1364/OE.22.010710.

[4] M. W. Geis *et al.*, "CMOS-compatible all-Si high-speed waveguide photodiodes with high responsivity in near-infrared communication band," *IEEE Photon. Technol. Lett.*, vol. 19, no. 3, pp. 152–154, Feb. 1, 2007, doi: 10.1109/LPT.2006.890109.

[5] S. Luryi, T. P. Pearsall, H. Temkin, and J. C. Bean, "Waveguide infrared photodetectors on a silicon chip," *IEEE Electron Device Lett.*, vol. 7, no. 2, pp. 104–107, Feb. 1986, doi: 10.1109/EDL.1986.26309.

[6] L. Alloatti and R. J. Ram, "Resonance-enhanced waveguide-coupled silicon-germanium detector," *Appl. Phys. Lett.*, vol. 108, p. 071105, Feb. 2016, doi: 10.1063/1.4941995.

[7] J.-F. Bourhis, "Fiber-to-waveguide connection," *Proc. SPIE*, vol. 10275, pp. 102750L-1–102750L-32, Jul. 1994.

[8] P. Karioja, J. Ollila, V.-P. Putila, K. Keranen, J. Hakkila, and H. Kopola, "Comparison of active and passive fiber alignment techniques for multimode laser pigtailing," in *Proc. 50th Electron. Compon. Technol. Conf.*, Las Vegas, NV, USA, May 2000, pp. 244–249.

[9] Y. Gao *et al.*, "Photon-trapping microstructures enable high-speed high-efficiency silicon photodiodes," *Nature Photon.*, vol. 11, pp. 301–308, Apr. 2017, doi: 10.1038/nphoton.2017.37.

[10] S.-F. Leung *et al.*, "Light management with nanostructures for optoelectronic devices," *J. Phys. Chem. Lett.*, vol. 5, pp. 1479–1495, Apr. 2014, doi: 10.1021/jz500306f.

[11] J. Q. Xi *et al.*, "Optical thin-film materials with low refractive index for broadband elimination of Fresnel reflection," *Nature Photon.*, vol. 1, no. 3, pp. 176–179, 2007, doi: 10.1038/nphoton.2007.26.

[12] P. Kuang, S. Eyderman, M.-L. Hsieh, A. Post, S. John, and S.-Y. Lin, "Achieving an accurate surface profile of a photonic crystal for near-unity solar absorption in a super thin-film architecture," *ACS Nano*, vol. 10, pp. 6116–6124, Jun. 2016, doi: 10.1021/acsnano.6b01875.

[13] S. Jeong, M. D. McGehee, and Y. Cui, "All-back-contact ultra-thin silicon nanocone solar cells with 13.7% power conversion efficiency," *Nature Commun.*, vol. 4, Dec. 2013, Art. no. 2950, doi: 10.1038/ncomms3950.

[14] K. J. Yu *et al.*, "Light trapping in ultrathin monocrystalline silicon solar cells," *Adv. Energy Mater.*, vol. 3, pp. 1401–1406, Jul. 2013, doi: 10.1002/aenm.201300542.

[15] M. S. Branham *et al.*, "15.7% efficient 10-*mu*m-thick crystalline silicon solar cells using periodic nanostructures," *Adv. Mater.*, vol. 27, pp. 2182–2188, Apr. 2015, doi: 10.1002/adma.201405511.

[16] H. Lin *et al.*, "Developing controllable anisotropic wet etching to achieve silicon nanorods, nanopencils and nanocones for efficient photon trapping," *J. Mater. Chem. A*, vol. 1, no. 34, pp. 9942–9946, Jun. 2013, doi: 10.1039/C3TA11889D.

[17] E. Garnett and P. Yang, "Light trapping in silicon nanowire solar cells," *Nano Lett.*, vol. 10, no. 3, pp. 1082–1087, Mar. 2010, doi: 10.1021/nl100161z.

[18] J. Zhu, C.-M. Hsu, Z. Yu, S. Fan, and Y. Cui, "Nanodome solar cells with efficient light management and self-cleaning," *Nano Lett*, vol. 10, pp. 1979–1984, Jun. 2010, doi: 10.1021/nl9034237.

[19] E. Yablonovitch and G. D. Cody, "Intensity enhancement in textured optical sheets for solar cells," *IEEE Trans. Electron Devices*, vol. 29, no. 2, pp. 300–305, Feb. 1982, doi: 10.1109/T-Ed.1982.20700.

[20] S. John, "Why trap light?" *Nature Mater.*, vol. 11, pp. 997–999, Dec. 2012, doi: 10.1038/nmat3503.

[21] S. E. Han and G. Chen, "Toward the Lambertian limit of light trapping in thin nanostructured silicon solar cells," *Nano Lett.*, vol. 10, no. 11, pp. 4692–4696, Oct. 2010, doi: 10.1021/nl1029804.

[22] Y. Zhou, M. Moewe, J. Kern, M. C. Y. Huang, and C. J. Chang-Hasnain, "Surface-normal emission of a high-Q resonator using a subwavelength high-contrast grating," *Opt. Exp.*, vol. 16, pp. 17282–17287, Oct. 2008, doi: 10.1364/OE.16.017282.

[23] P. Spinelli, M. A. Verschuuren, and A. Polman, "Broadband omnidirectional antireflection coating based on subwavelength surface Mie resonators," *Nature Commun.*, vol. 3, Feb. 2012, Art. no. 692, doi: 10.1038/ncomms1691.

[24] S. Fan and J. D. Joannopoulos, "Analysis of guided resonances in photonic crystal slabs," *Phys. Rev. B, Condens. Matter*, vol. 65, no. 23, p. 235112, 2002, doi: 10.1103/PhysRevB.65.235112.

[25] J. L. Donnelly *et al.*, "Mode-based analysis of silicon nanohole arrays for photovoltaic applications," *Opt. Exp.*, vol. 22, no. S5, pp. A1343–A1354, Aug. 2014, doi: 10.1364/Oe.22.0a1343.

[26] Z. Yu, A. Raman, and S. Fan, "Fundamental limit of nanophotonic light trapping in solar cells," *Proc. Nat. Acad. Sci. USA*, vol. 107, pp. 17491–17496, Oct. 2010, doi: 10.1073/pnas.1008296107.

[27] S. Peng and G. M. Morris, "Resonant scattering from two-dimensional gratings," *J. Opt. Soc. Amer. A, Opt. Image Sci.*, vol. 13, no. 5, pp. 993–1005, 1996, doi: 10.1364/JOSAA.13.000993.

[28] B. C. P. Sturmberg *et al.*, "Modal analysis of enhanced absorption in silicon nanowire arrays," *Opt. Exp.*, vol. 19, pp. A1067–A1081, Jul. 2011, doi: 10.1364/OE.19.0A1067.

[29] K. Sakoda, "Enhanced light amplification due to group-velocity anomaly peculiar to two-and three-dimensional photonic crystals," *Opt. Exp.*, vol. 4, pp. 167–176, Mar. 1999, doi: 10.1364/OE.4.000167.

[30] S. Eyderman, S. John, and A. Deinega, "Solar light trapping in slanted conical-pore photonic crystals: Beyond statistical ray trapping," *J. Appl. Phys.*, vol. 113, p. 154315, Apr. 2013, doi: 10.1063/1.4802442.

[31] X. Zhang, Y. Yu, J. Xi, Y. Wang, and X.-H. Sun, "Absorption enhancement in double-sided nanocone hole arrays for solar cells," *J. Opt.*, vol. 17, p. 075901, Jun. 2015, doi: 10.1088/2040-8978/17/7/075901.

[32] X. Ziang, W. Wei, Q. Laixiang, X. Wanjin, and G. G. Qin, "Optical absorption characteristics of nanometer and submicron a-Si:H solar cells with two kinds of nano textures," *Opt. Exp.*, vol. 21, pp. 18043–18052, Jul. 2013, doi: 10.1364/OE.21.018043.

[33] Z. Xia, X. Qin, Y. Wu, Y. Pan, J. Zhou, and Z. Zhang, "Efficient broadband light absorption in elliptical nanohole arrays for photovoltaic application," *Opt. Lett.*, vol. 40, pp. 5814–5817, Dec. 2015, doi: 10.1364/OL.40.005814.

[34] C. Lin and M. L. Povinelli, "Optimal design of aperiodic, vertical silicon nanowire structures for photovoltaics," *Opt. Exp.*, vol. 19, pp. A1148–A1154, Sep. 2011, doi: 10.1364/OE.19.0A1148.

[35] U. Paetzold *et al.*, "Disorder improves nanophotonic light trapping in thin-film solar cells," *Appl. Phys. Lett.*, vol. 104, p. 131102, Mar. 2014, doi: 10.1063/1.4869289.

[36] A. S. Mayet *et al.*, "Inhibiting device degradation induced by surface damages during top-down fabrication of semiconductor devices with micro/nano-scale pillars and holes," *Proc. SPIE*, vol. 9924, pp. 99240C-1–99240C-7, Sep. 2016.

[37] K. Zang *et al.*, "Silicon single-photon avalanche diodes with nanostructured light trapping," *Nature Commun.*, vol. 8, Sep. 2017, Art. no. 628, doi: 10.1038/s41467-017-00733-y.

[38] C. Soci, A. Zhang, X. Y. Bao, H. Kim, Y. Lo, and D. Wang, "Nanowire photodetectors," *J. Nanosci. Nanotechnol.*, vol. 10, pp. 1430–1449, Mar. 2010, doi: 10.1166/jnn.2010.2157.

[39] C. Yan and P. S. Lee, "Recent progresses in improving nanowire photodetector performances," *Sci. Adv. Mater.*, vol. 4, pp. 241–253, Feb. 2012, doi: 10.1166/sam.2012.1280.

[40] V. J. Logeeswaran *et al.*, "A perspective on nanowire photodetectors: Current status, future challenges, and opportunities," *IEEE J. Sel. Topics Quantum Electron.*, vol. 17, no. 4, pp. 1002–1032, Jul./Aug. 2011, doi: 10.1109/Jstqe.2010.2093508.

[41] T. Zhai *et al.*, "A comprehensive review of one-dimensional metal-oxide nanostructure photodetectors," *Sensors*, vol. 9, pp. 6504–6529, Aug. 2009, doi: 10.3390/s90806504.

[42] R. R. LaPierre, M. Robson, K. M. Azizur-Rahman, and P. Kuyanov, "A review of III–V nanowire infrared photodetectors and sensors," *J. Phys. D, Appl. Phys.*, vol. 50, p. 123001, Feb. 2017, doi: 10.1088/1361-6463/aa5ab3.

[43] V. J. Logeeswaran *et al.*, "A 14-ps full width at half maximum high-speed photoconductor fabricated with intersecting InP nanowires on an amorphous surface," *Appl. Phys. A, Solids Surf.*, vol. 91, pp. 1–5, Apr. 2008, doi: 10.1007/s00339-007-4394-x.

[44] M. S. Islam, S. Sharma, T. Kamins, and R. S. Williams, "A novel interconnection technique for manufacturing nanowire devices," *Appl. Phys. A, Solids Surf.*, vol. 80, pp. 1133–1140, Mar. 2005, doi: 10.1007/s00339-004-3177-x.

[45] M. S. Islam, S. Sharma, T. Kamins, and R. S. Williams, "Ultrahigh-density silicon nanobridges formed between two vertical silicon surfaces," *Nanotechnology*, vol. 15, p. L5, Jan. 2004, doi: 10.1088/0957-4484/15/5/L01.

[46] E. M. Gallo *et al.*, "Picosecond response times in GaAs/AlGaAs core/shell nanowire-based photodetectors," *Appl. Phys. Lett.*, vol. 98, p. 241113, Jun. 2011, doi: 10.1063/1.3600061.

[47] M. Seyedi, M. Yao, J. O'Brien, S. Y. Wang, and P. D. Dapkus, "Efficient Schottky-like junction GaAs nanowire photodetector with 9 GHz modulation bandwidth with large active area," *Appl. Phys. Lett.*, vol. 105, p. 041105, Jul. 2014, doi: 10.1063/1.4891764.

[48] A. C. Farrell *et al.*, "Plasmonic field confinement for separate absorption-multiplication in InGaAs nanopillar avalanche photodiodes," *Sci. Rep.*, vol. 5, Dec. 2015, Art. no. 17580, doi: 10.1038/srep17580.

[49] S. Muehlbrandt *et al.*, "Silicon-plasmonic internal-photoemission detector for 40 Gbit/s data reception," *Optica*, vol. 3, pp. 741–747, Jul. 2016, doi: 10.1364/OPTICA.3.000741.

[50] F. Wang and N. A. Melosh, "Plasmonic energy collection through hot carrier extraction," *Nano Lett.*, vol. 11, pp. 5426–5430, Oct. 2011, doi: 10.1021/nl203196z.

[51] L. Du, A. Furube, K. Hara, R. Katoh, and M. Tachiya, "Ultrafast plasmon induced electron injection mechanism in gold–TiO_2 nanoparticle system," *J. Photochem. Photobiol. C, Photochem. Rev.*, vol. 15, pp. 21–30, Jun. 2013, doi: 10.1016/j.jphotochemrev.2012.11.001.

[52] W. Li and G. Valentine Jason, "Harvesting the loss: surface plasmon-based hot electron photodetection," *Nanophotonics*, vol. 6, pp. 177–191, Nov. 2017, doi: 10.1515/nanoph-2015-0154.

[53] H. A. Atwater and A. Polman, "Plasmonics for improved photovoltaic devices," *Nature Mater.*, vol. 9, pp. 205–213, Feb. 2010, doi: 10.1038/nmat2629.

[54] C. Sönnichsen *et al.*, "Drastic reduction of plasmon damping in gold nanorods," *Phys. Rev. Lett.*, vol. 88, p. 077402, Jan. 2002, doi: 10.1103/PhysRevLett.88.077402.

[55] A. Sobhani *et al.*, "Narrowband photodetection in the near-infrared with a plasmon-induced hot electron device," *Nature Commun.*, vol. 4, Mar. 2013, Art. no. 1643, doi: 10.1038/ncomms2642.

[56] Y. K. Lee, C. H. Jung, J. Park, H. Seo, G. A. Somorjai, and J. Y. Park, "Surface plasmon-driven hot electron flow probed with metal-semiconductor nanodiodes," *Nano Lett.*, vol. 11, pp. 4251–4255, Oct. 2011, doi: 10.1021/nl2022459.

[57] P. Narang, R. Sundararaman, and A. Atwater Harry, "Plasmonic hot carrier dynamics in solid-state and chemical systems for energy conversion," *Nanophotonics*, vol. 5, pp. 96–111, Jun. 2016, doi: 10.1515/nanoph-2016-0007.

[58] T. Ishi, J. Fujikata, K. Makita, T. Baba, and K. Ohashi, "Si nano-photodiode with a surface plasmon antenna," *Jpn. J. Appl. Phys.*, vol. 44, p. L364, Nov. 2005, doi: 10.1143/JJAP.44.L364.

[59] I. Goykhman *et al.*, "On-chip integrated, silicon–graphene plasmonic Schottky photodetector with high responsivity and avalanche photogain," *Nano Lett.*, vol. 16, pp. 3005–3013, Apr. 2016, doi: 10.1021/acs.nanolett.5b05216.

[60] U. Levy, M. Grajower, P. A. D. Gonçalves, N. A. Mortensen, and J. B. Khurgin, "Plasmonic silicon Schottky photodetectors: The physics behind graphene enhanced internal photoemission," *APL Photon.*, vol. 2, p. 026103, Jan. 2017, doi: 10.1063/1.4973537.

[61] H. Jalili and O. Momeni, "A 0.34-THz varactor-less scalable standing wave radiator array with 5.9% tuning range in 130 nm BiCMOS," in *Proc. IEEE Radio Freq. Integr. Circuits Symp. (RFIC)*, San Francisco, CA, USA, May 2016, pp. 182–185.

[62] H. Jalili and O. Momeni, "A 318-to-370 GHz standing-wave 2D phased array in 0.13 μm BiCMOS," in *IEEE Int. Solid-State Circuits Conf. (ISSCC) Dig. Tech. Papers*, San Francisco, CA, USA, Feb. 2017, pp. 310–311.

[63] M. L. Brongersma, N. J. Halas, and P. Nordlander, "Plasmon-induced hot carrier science and technology," *Nature Nanotechnol.*, vol. 10, pp. 25–34, Jan. 2015, doi: 10.1038/nnano.2014.311.

[64] T. Baba, "Slow light in photonic crystals," *Nature Photon.*, vol. 2, no. 8, pp. 465–473, 2008, doi: 10.1038/nphoton.2008.146.

[65] P. Russell, "Photonic crystal fibers," *Science*, vol. 299, no. 5605, pp. 358–362, Jan. 2003, doi: 10.1126/science.1079280.

[66] H. Cansizoglu *et al.*, "Efficient Si photovoltaic devices with integrated micro/nano holes," *Proc. SPIE*, vol. 9924, pp. 99240V-1–99240V-6, Sep. 2016.

[67] S.-W. Chung, J.-Y. Yu, and J. R. Heath, "Silicon nanowire devices," *Appl. Phys. Lett.*, vol. 76, pp. 2068–2070, Apr. 2000, doi: 10.1063/1.126257.

[68] A. Chaudhry, V. Ramamurthi, E. Fong, and M. S. Islam, "Ultra-low contact resistance of epitaxially interfaced bridged silicon nanowires," *Nano Lett.*, vol. 7, pp. 1536–1541, 2007.

[69] M. Yoshimura, E. Nakai, K. Tomioka, and T. Fukui, "Indium tin oxide and indium phosphide heterojunction nanowire array solar cells," *Appl. Phys. Lett.*, vol. 103, p. 243111, Dec. 2013, doi: 10.1063/1.4847355.

[70] H. Cansizoglu, M. F. Cansizoglu, F. Watanabe, and T. Karabacak, "Enhanced photocurrent and dynamic response in vertically aligned In_2S_3/Ag core/shell nanorod array photoconductive devices," *ACS Appl. Mater. Interfaces*, vol. 6, pp. 8673–8682, May 2014, doi: 10.1021/am501481w.

[71] Y. Gao *et al.*, "A high speed surface illuminated Si photodiode using microstructured holes for absorption enhancements at 900–1000 nm wavelength," *ACS Photon.*, vol. 4, pp. 2053–2060, Jul. 2017, doi: 10.1021/acsphotonics.7b00486.

[72] R. Rasshofer, M. Spies, and H. Spies, "Influences of weather phenomena on automotive laser radar systems," *Adv. Radio Sci.*, vol. 9, pp. 49–60, Jul. 2011, doi: 10.5194/ars-9-49-2011.

[73] R. Baca, P. Kolesar, J. Tatum, D. Gazula, E. Shaw, and T. Gray, "Advances in multimode fiber transmission for the data center," in *Proc. Opt. Fiber Commun. Conf. Exhibit. (OFC)*, Los Angeles, CA, USA, 2015, p. 1–3.

[74] F. Chang *et al.*, "First demonstration of PAM4 transmissions for record reach and high-capacity SWDM links over MMF using 40G/100G PAM4 IC chipset with real-time DSP," in *Proc. Opt. Fiber Commun. Conf. Exhibit. (OFC)*, Los Angeles, CA, USA, 2017, pp. 1–3.

[75] D. Lewis and J. King, "100G SWDM4 MSA technical specifications," Finisar, Sunnyvale, CA, USA, Tech. Rep., 2017. [Online]. Available: http://www.swdm.org/wp-content/uploads/2017/03/100G-SWDM4-MSA-Technical-Spec-Rev2.pdf

[76] Y. Sun *et al.*, "SWDM PAM4 transmission over next generation wideband multimode optical fiber," *J. Lightw. Technol.*, vol. 35, pp. 690–697, Feb. 15, 2017, doi: 10.1109/jlt.2016.2618723.

[77] M. R. Tan, P. Rosenberg, W. Sorin, S. Mathai, G. Panotopoulos, and G. Rankin, "Universal photonic interconnect for data centers," in *Proc. Opt. Fiber Commun. Conf. (OFC)*, Los Angeles, CA, USA, 2017, pp. 1–3.

[78] M. A. Taubenblatt, "Optical interconnects for high-performance computing," *J. Lightw. Technol.*, vol. 30, pp. 448–457, Feb. 15, 2012, doi: 10.1109/JLT.2011.2172989.

[79] D. Kuchta, "High-Capacity VCSEL Links," in *Proc. Opt. Fiber Commun. Conf.*, Los Angeles, CA, USA, 2017, pp. 1–94.

[80] V. Houtsma, D. van Veen, and E. Harstead, "Recent progress on standardization of next-generation 25, 50, and 100G EPON," *J. Lightw. Technol.*, vol. 35, pp. 1228–1234, Mar. 15, 2016, doi: 10.1109/JLT.2016.2637825.

[81] A. McCarthy *et al.*, "Kilometer-range depth imaging at 1550 nm wavelength using an InGaAs/InP single-photon avalanche diode detector," *Opt. Exp.*, vol. 21, no. 19, pp. 22098–22113, Sep. 2013, doi: 10.1364/OE.21.022098.

[82] M. Ren *et al.*, "Laser ranging at 1550 nm with 1-GHz sine-wave gated InGaAs/InP APD single-photon detector," *Opt. Exp.*, vol. 19, no. 14, pp. 13497–13502, 2011, doi: 10.1364/OE.19.013497.

[83] R. H. Hadfield, "Single-photon detectors for optical quantum information applications," *Nature Photon.*, vol. 3, no. 12, pp. 696–705, Dec. 2009, doi: 10.1038/nphoton.2009.230.

Hilal Cansizoglu (M'17) received the M.S. degree in electrical engineering from Southern Methodist University, Dallas, TX, USA, 2010, and the Ph.D. degree in applied physics from the University of Arkansas at Little Rock, Little Rock, AR, USA, in 2014.

She is a Post-Doctoral Fellow with the Department of Electrical and Computer Engineering, University of California at Davis, Davis, CA, USA. She is currently working on CMOS-compatible high speed Si photodiodes.

Ekaterina Ponizovskaya Devine received the M.S. and Ph.D. degrees from the Moscow Institute of Physics and Technology (State University), Moscow, Russia, in 1999.

She was with the Ames Center, NASA, Mountain View, CA, USA, where she was involved in the optimization and physics-based models for prognostics and automation. She is currently with W&WSens Device, Inc., Los Altos, CA, USA, where she is focusing on photonics and photodetectors.

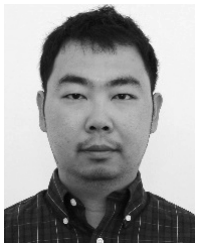

Yang Gao received the B.S and M.S degrees from the Harbin Institute of Technology, Harbin, China, in 2006 and 2008, respectively, and the Ph.D. degree in mechanical engineering from the State University of New York, Binghamton, NY, USA, in 2013.

He is currently a Post-Doctoral Scholar with the University of California, Davis, CA, USA.

Soroush Ghandiparsi received the B.Sc. degree in electrical engineering and the M.Sc. degree in nanophotonic engineering from the School of Engineering Emerging Technology, Sharif University of Technology, Tehran, Iran, in 2009 and 2012, respectively. He is currently pursuing the Ph.D. degree with the Integrated Nano and Micro Systems Group, Department of Electrical and Computer Engineering, UC Davis, Davis, CA, USA.

He is currently involved in high-speed short-reach optical communication project.

Toshishige Yamada (SM'11) received the B.S. and M.S. degrees in physics from The University of Tokyo, Tokyo, Japan, and the Ph.D. degree in electrical engineering from Arizona State University, Tempe, AZ, USA.

He joined the NASA Ames Research Center, Moffett Field, CA, USA. He is currently with the University of California at Santa Cruz, Santa Cruz, CA, USA.

Aly F. Elrefaie (M'83–SM'86–F'04) received the B.S.E.E. degree (Hons.) from Ain Shams University, Cairo, Egypt, in 1976, and the M.Sc. and Ph.D. degrees in electrical engineering from NYU, Brooklyn, NY, USA, in 1980 and 1983, respectively.

Since 2014, he has been a Chief Scientist with W&Wsens Devices, Inc., Los Altos, CA, USA, where he is focusing on topics related to nano technology in optical communications.

Shih-Yuan (SY) Wang (LF'12) received the B.S. degree in engineering physics and the Ph.D. degree in electrical engineering and computer sciences from the University of California at Berkeley, Berkeley, CA, USA, in 1969 and 1977, respectively.

He is currently with W&WSens Devices, Inc., Los Altos, CA, USA, where he is involved in silicon photodiodes compatible with CMOS process and integration for data center interconnect applications.

M. Saif Islam (SM'15) received the B.Sc. degree in physics from Middle East Technical University, Ankara, Turkey, in 1994, the M.S. degree in physics from Bilkent University, Ankara, in 1996, and the Ph.D. degree in electrical engineering from UCLA, Los Angeles, CA, USA, in 2001.

He joined the University of California, Davis, CA, USA, in 2004, where he is currently a Professor.